SANDIA REPORT

2012-7736
Unlimited Release
Printed October 2012

The Fundamentals of Plastic Deformation: Several Case Studies of Plasticity in Confined Volumes

Christopher R. Weinberger

Prepared by
Sandia National Laboratories
Albuquerque, New Mexico 87185 and Livermore, California 94550

Sandia National Laboratories is a multi-program laboratory managed and operated by Sandia Corporation, a wholly owned subsidiary of Lockheed Martin Corporation, for the U.S. Department of Energy's National Nuclear Security Administration under contract DE-AC04-94AL85000.

Approved for public release; further dissemination unlimited.

Sandia National Laboratories

Issued by Sandia National Laboratories, operated for the United States Department of Energy by Sandia Corporation.

NOTICE: This report was prepared as an account of work sponsored by an agency of the United States Government. Neither the United States Government, nor any agency thereof, nor any of their employees, nor any of their contractors, subcontractors, or their employees, make any warranty, express or implied, or assume any legal liability or responsibility for the accuracy, completeness, or usefulness of any information, apparatus, product, or process disclosed, or represent that its use would not infringe privately owned rights. Reference herein to any specific commercial product, process, or service by trade name, trademark, manufacturer, or otherwise, does not necessarily constitute or imply its endorsement, recommendation, or favoring by the United States Government, any agency thereof, or any of their contractors or subcontractors. The views and opinions expressed herein do not necessarily state or reflect those of the United States Government, any agency thereof, or any of their contractors.

Printed in the United States of America. This report has been reproduced directly from the best available copy.

Available to DOE and DOE contractors from
U.S. Department of Energy
Office of Scientific and Technical Information
P.O. Box 62
Oak Ridge, TN 37831

Telephone: (865) 576-8401
Facsimile: (865) 576-5728
E-Mail: reports@adonis.osti.gov
Online ordering: http://www.osti.gov/bridge

Available to the public from
U.S. Department of Commerce
National Technical Information Service
5285 Port Royal Rd
Springfield, VA 22161

Telephone: (800) 553-6847
Facsimile: (703) 605-6900
E-Mail: orders@ntis.fedworld.gov
Online ordering: http://www.ntis.gov/help/ordermethods.asp?loc=7-4-0#online

2012-7736
Unlimited Release
Printed October 2012

The Fundamentals of Plastic Deformation: Several Case Studies of Plasticity in Confined Volumes

Christopher R. Weinberger
Computational Materials Science and Engineering Department
Sandia National Laboratories
P.O. Box 5800
Albuquerque, NM 87185-1411
crweinb@sandia.gov

Abstract

Plasticity in small volumes is significantly different than in large, bulk-like specimens. The strength of materials in the micron and sub-micron regime depends not only on the microstructure but also on the size of the material. Given that a number of important mechanical processes occur at these length scales, it is important to build a comprehensive understanding of these materials and processes. This work examines several different processes in small volumes. The motion of dislocations in the drag regime are examined as a function of material volume which exhibits higher drag than in the bulk. The stability of single arm sources are also investigated using molecular dynamics. Finally, dislocation nucleation from the free surface is investigated using both atomistic as well as continuum models. These results provide a better understanding of plastic processes in confined volumes.

Acknowledgment

The author would like to thank a number of people who contributed to the work on this project including Dr. Andrew T. Jennings (formerly at Cal Tech, now BCG), Prof. Wei Cai (Stanford) and Prof. Julia R. Greer (Cal Tech). A number of Sandian's also contributed to the success of this work in a variety of ways including my mentor Dr. Stephen Foiles (Org. 1814), Dr. Corbett Battaile (Org. 1814) and Dr. Garritt Tucker (Org. 1814).

This research was supported in part by an appointment to the Sandia National Laboratories Truman Fellowship in National Security Science and Engineering, sponsored by Sandia Corporation (a wholly owned subsidiary of Lockheed Martin Corporation) as Operator of Sandia National Laboratories under its U.S. Department of Energy Contract No. DE-AC04-94AL85000.

Contents

Nomenclature **9**

1 Introduction **11**

2 Background **13**

Micropillars 14

3 Dislocation Motion and Stability in Confined Volumes **17**

Dislocation Drag at the Nanoscale 17

The Stability of Dislocation Pinning Points 20

4 Dislocation Nucleation From Free Surfaces **23**

Atomistics Simulations of Dislocation Nucleation 24

Continuum Models for Predicting Nucleation Strengths 27

Bulk Nucleation 28

Half Space Nucleation 28

5 Conclusion **31**

References **32**

List of Figures

2.1 A hypothetical dislocation microstructure is shown in (a) prior to creating a pillar out of it as shown in (b). These views are two-dimensional and for illustrative purposes but schematically show the removal of a non-representative volume of defects from a larger volume. 15

3.1 An edge dislocation in FCC nickel. The thickness of the thin film is along the $y-$direction and the film (and dislocation length) are along the $z-$direction. Bulk-like simulations are carried out with the $z-$direction under periodic boundary conditions, which are not illustrated here. Reprinted with permission from [72]. 18

3.2 A double ended source pinned by a Lomer-Cottrell jog in a 50 nm diameter copper nanopillar. (a) The initial source created by a cut and weld procedure after a short energy minimization. The pillar lies along the $\langle 100 \rangle$ direction in the FCC crystal. The long dislocation segments have a Burgers vector of $\frac{a}{2}\langle 110 \rangle$. The Lomer-Cottrell jog has the same Burgers vector, however, due to its line direction, it must glide on a $\{100\}$ glide plane. (b) Under the applied loads the mobile arms begin to rotate and the Lomer-Cottrell jog dissociates and pins the dislocation. (b)-(c) As the dislocation rotates, the Lomer-Cottrell segment constricts allowing the dislocation to glide on its $\{100\}$ plane and (d) eventually drifts out of the pillar. . . 21

4.1 (a) The energy barrier and computed for a ~ 5 nm gold nanowire with a rhombic cross-section under a uniaxial compressive stress of approximately 2.6 GPa. (b)-(g) Snapshots of the nucleation process at 2.6 GPa. The subfigure labels correspond to the labels on the curve in (a). 25

4.2 The energy barriers of the five different nanowires in tension and compression. (a) Energy barrier curves for the $\langle 100 \rangle$ nanowires in compression. (b) Energy barrier curves for the $\langle 100 \rangle$ nanowires in tension. (c) Energy barrier curves for the $\langle 110 \rangle$ nanowires in compression. (d) Energy barrier curves for the $\langle 110 \rangle$ nanowires in tension. Note that the stress values are corrected for the surface stress and are thus representative of large diameter nanowires. The data points represent the data from atomistics and the lines represent curve fits. 26

4.3 The strength predicted from the atomistic simulations as compared against experimental measurements of the flow stress in (a) compression and (a) tension of gold micro- and nano-pillars. 27

4.4 The pristine nucleation strength of single crystal FCC metals resolved onto their slip planes compared to the resolved flow strengths from micropillar compression tests. 30

List of Tables

4.1 A comparison of the predicted strengths of large ~ 100 nm diameter gold nanowires as compared to experiments. 25

4.2 The inner core radius, r_c determined from fitting the model homogeneous partial dislocation nucleation to atomistic data. 29

Nomenclature

DD Discrete Dislocation Dynamics

MD Molecular Dynamics

FIB Focus Ion Beam

FCC Face Centered Cubic

BCC Body Centered Cubic

SSD Statistically Stored Dislocation

GND Geometrically Necessary Dislocation

EAM Embedded Atom Method

Chapter 1

Introduction

It is well established that strength in many crystalline materials, most notably metals, is controlled by the motion and interaction of dislocations. In conventional engineering metals, the volume of material and grain size in these materials allow for a large representative distribution of these defects. This results in a mechanical response that is often observed to be independent of the size of the specimen. Thus, material strength, such as the ultimate tensile strength, is often described as an intensive property of the material.

There are many applications in which the volume of the material being tested may not contain enough defects to be representative, which results in the properties of the material, such as strength, to no longer be intensive. For example, the friction properties of metals is dependent on the evolving microstructure under the wear track [4, 5, 59]. The microstructure that develops is typical several hundred nanometers in depth. To understand the mechanical properties of wear track microstructures, mechanical testing of small volumes are required. Similarly, small scale mechanical testing can be used to determine the strength of irradiated materials [28]. The depth of damage in these materials is very small, typically a few microns, for short irradiation times which are used as part of research and development in this area [28]. Thus, understanding mechanical properties at small scales is very important for these studies and tools to be useful in engineering design.

This report discusses several aspects of plasticity in confined volumes. First, we investigate how dislocations move in small volumes using molecular dynamics simulations. Specifically, the surfaces on the drag of dislocations is investigated as well as the stability of pinning points in nanopillars. Dislocation nucleation, which can be a dominant source of plasticity in nanoscale metals, is also investigated using atomistic simulations. A continuum model of dislocation motion is formulated that is based on matching atomistic simulations.

Chapter 2

Background

Plasticity in confined volumes has been an intense area of research in mechanical properties over the last 15 years [22, 38, 69]. The interest in this field began with the experiments by Fleck *et al.* [17–19] on the torsion of small diameter wires. These experiments reported that the sustained torsional moment during plastic deformation depended strongly on the diameter of the wire. Since, as previously mentioned, strength is supposed to be an intensive property and thus not dependent on size, these experimental results were quite surprising. This lead to the development of the idea of strain gradient plasticity [17–19, 21, 26, 27, 31, 40].

Strain gradient plasticity, now a well developed field, asserts that the presence of strain gradients induced by the applied load results in geometrically necessary dislocations that help strengthen the material. The theory assumes the flow stress is proportional to the square root of the dislocation density: $\tau = \alpha\mu b\sqrt{\rho}$ where τ is the flow stress, μ is the shear modulus, b is the Burgers vector, ρ is the dislocation density and α is a constant of proportionality. The dislocation density is then assumed to have contributions from statistically stored dislocations (SSDs) and geometrically necessary dislocations (GNDs), $\rho = \rho_{\text{SSD}} + \rho_{\text{GND}}$. The strain gradients imposed in the material, and hence the induced GNDs, increased with a decrease in material size. Thus, smaller materials will exhibit stronger flow strengths.

Similar to size effects observed in the torsion of small scale wires, size effects have also been reported in nano-indentation. The identation size effect [3, 13, 25, 36, 52, 58, 62] appears as an increase in hardness with a decrease in indentation depth. This size-effect was initially explained using strain gradient plasticity in the classic model of Nix and Gao [52]. This model assumes that GNDs must form under the indentor during plastic deformation and lead to a hardness-depth relationship of $H = H_o\sqrt{1+d^*/d}$, where d is the depth, d^* is a characteristic length scale and H_o is the hardness at deep indents. Despite the success of this model in its ability to capture the experimental trends, recent work has called this model into question. Detailed electron backscatter diffraction (EBSD) work has not shown high dislocation densities below the indentor, which would be required under the assumptions of the Nix-Gao model. These results are supported by other experiments as well as discrete dislocation dynamics simulations of the indentation process. An alternative interpretation that has emerged of the indentation size effect is that it is a result of source limited deformation [39, 58].

Micropillars

The idea of source limited deformation originates in attempts to understand the observed size effects in micropillars. The pioneering work of Uchic *et al.* [68] showed that the flow stress of single crystal nickel pillars depended on the size of the material when the diameter was reduced below a critical diameter, here about 25 μm. These pillars were machined using a focus ion beam (FIB) and were subsequently compressed by a flat indentor. The results of this work are critical to developing an understanding of plasticity in confined volumes because it demonstrates that size effects exist even in the absence of strain gradients.

The work by Uchic *et al.* [68] led to an enormous effort to characterize and understand this new size effect. One of the key results from the experimental efforts is the appearance of a universal size effect amongst face-centered-cubic (FCC) single crystals. This universal scaling law states that the flow strength of the metal scales has a power law dependence on the pillar diameter [22, 38, 69], $\sigma \sim D^{-0.6}$. The development of tensile experiments at the micron and submicron scale confirm the size effect exists in tension as well as compression.

Another important observed trend in the experiments is the effects of pre-strain on the mechanical behavior of these small samples. For example, Bei *et al.* [30] have shown that increased pre-strian in their pillars actually makes them softer. This suggests that adding defects in the pillars makes them weaker, in direct contrast to bulk behavior where strain hardening is typically observed. Similarly, Lee *et al.* [41] confirmed the results of Bei *et al.* [30] that adding defects made the pillars weaker but also showed that annealing made the pillars stronger. Again, this suggests that plasticity in these small scale pillars is much different than those of bulk materials.

Efforts to understand the size effect including the universal scaling law, has resulted in many different theories. The initial focus was in understanding the potential influence of the FIB damage. Since the FIB process may induce a large amount of damage on the surface, this has the potential to trap dislocations on the interior of the pillar and harden the material. However, the mountain of evidence does not support a significant influence of the FIB damage. For example, the work by Greer and Nix [23] initially used electroplating to create gold pillars and showed similar flow stresses as the FIBed pillars. This idea was later reinvestigated by Jennings *et al.* [32] using electroplated copper pillars who showed that the size effect in their pillars is the same as those in FIBed pillars. Similar results were obtained by comparing gold pillars created using an embossing technique when compared to pillars created using the FIB [15]. Thus, it appears that the FIB damage itself is not responsible for the observed size effects.

Since the size of these pillars are quite small, one prominent theory that has been used to explain the size effect is the emergence of dislocation nucleation from the free surface [23, 53]. This idea was originally proposed by Greer and Nix [23] as part of the dislocation starvation hypothesis. The idea behind dislocation starvation is the idea that mobile dislocations in small volumes have a significantly higher probability of annihilation at the free surface. The depletion of mobile dislocations, termed dislocation starvation, leads to activation of additional sources in the pillars. Numerous theoretical studies have set out to provide a basis for the observed strengthening. However, a well accepted theory that includes dislocation nucleation has not been developed that

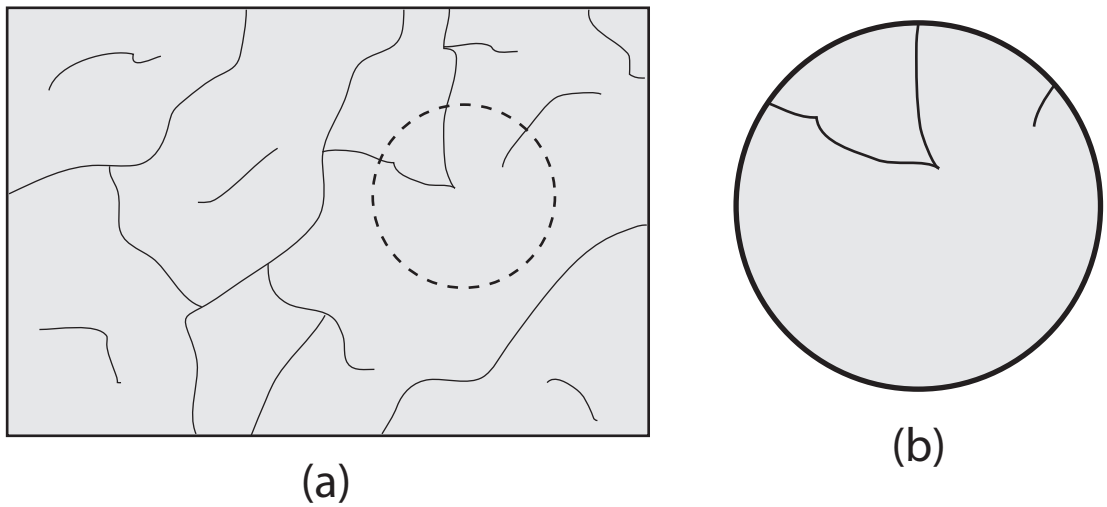

Figure 2.1. A hypothetical dislocation microstructure is shown in (a) prior to creating a pillar out of it as shown in (b). These views are two-dimensional and for illustrative purposes but schematically show the removal of a non-representative volume of defects from a larger volume.

reproduces the experimentally observed size effect.

The most widely accepted theory of the observed size effect is the idea of source truncation hardening. In this model, originally proposed by Parasatharthy *et al.* [57], states that the dislocation sources that control plasticity are truncated Frank-Read sources in these small volumes. This is schematically shown in Figure 1; Figure 1(a) shows a schematic of a dislocation network in a bulk sample while Figure 2(b) shows the potential creation of sources in a pillar cut out of the bulk material. The simplest model of the strength of these sources is to assume the stress required to operate them scales inversely with the shortest distance between the pinning point and the free surface. This can be written analytically as $\tau = \frac{\mu b}{2\pi L}$. Using this simple idea and a statistical distribution of sources with a background stress of $\tau = \frac{\mu b}{2}\sqrt{\rho}$, the authors [57] were able to show their model reproduced the size effect very well.

This idea has been expanded upon using discrete dislocation dynamics [16, 44, 49, 60, 61, 65, 67]. The advantage of discrete dislocation dynamics over analytical models is the code tracks the complete evolution of the dislocation ensemble, not just a hypothetical yield or flow stress predicted by the simple model. Thus, discrete dislocation dynamics can produce not only size dependent strengths but it can also predict the flow stress evolution and hardening. Numerous studies have shown that these models reproduce not only the essential size effect on strength, but also demonstrate the effects of dislocation density on strength in agreement with experiments. Additionally, these models show a new mechanism of hardening in FCC metals: exhaustion hardening. This ideas was originally proposed for stage 0 hardening in BCC metals where it describes the

easy exhaustion of edge dislocations. Exhaustion hardening in FCC micropillars describes how the material strengthens as weaker (and hence longer) sources operate first and eventually exhaust causing the required stress for deformation to increase.

However, discrete dislocation dynamics rely on a number of untested assumptions. Many of the original simulations assumed that there were a number of hard fixed pinning points inside the pillar. One obvious consequence of this assumption is that the pinning points cannot be dissolved during the simulation, regardless of the subsequent dislocation evolution that occurs. Hence, the number of pinning points in the pillar can only go up during straining. Later simulations focused on relaxing this assumption allowing pinning points to form naturally. One of the most comprehensive studies is by Motz *et al.* [49] who show that the pinning points that form are created by junctions, most notably of the Lomer-Cottrell type. However, these types of stable pinning points still required assumptions of the mobility of the pinning segments, such as Lomer-Cottrell dislocations, whose stability at these high stresses and small sizes is unknown.

Chapter 3

Dislocation Motion and Stability in Confined Volumes

As discussed in the Background, the two predominant theories attempting to explain the micropillar size effect are dislocation nucleation and single arm sources. However, there have been a number of theories that have emerged to explain the size effects. The idea of FIB damage has continuously been used and refuted as an explanation of the size effect. Also, there has been mention that the surface steps created on the free surface, related to surface energy, may contribute significantly to strength. All of these theories, however, rely on the a basic understanding of the motion and stability of dislocation sources in small volumes. In this chapter, we investigate the motion and stability of dislocations in small volumes and the resulting effects on mechanical properties.

Dislocation Drag at the Nanoscale

Dislocation motion is usually described by the rate limiting process. For materials with high lattice resistance, such as ceramics and BCC metals at low temperatures, dislocation mobility is often controlled by thermally activated motion of the dislocation over the Peierls potential. In materials with a a large density of obstacles, such as dislocation motion in most closed-packed metals, the velocity of the dislocation is controlled by the mean breakaway time from obstacles and mean obstacle spacing [50]. However, in materials with low lattice resistance, the motion of dislocations in obstacle free environments is controlled by drag.

The equation of motion for a general dislocation line per-unit-length can be written as:

$$\frac{\mathrm{d}}{\mathrm{d}t}\left(m\frac{\mathrm{d}x}{\mathrm{d}t}\right) = -B\frac{\mathrm{d}x}{\mathrm{d}t} + \tau b \tag{3.1}$$

where m is the dislocation mass, B is the drag coefficient and τ is the resolved applied shear stress. The last term is the applied force on the dislocation and can be more generally obtained from the Peach-Koehler formula: $\mathbf{f} = \sigma \cdot \mathbf{b} \times \xi$ where σ is the full applied stress tensor, $\mathbf{b}$ is the Burgers vector and ξ is the dislocation line direction. During steady state motion of a dislocation line, the drag coefficient can be determined by a simple balance of forces: $Bv = \tau b$. Thus, if the dislocation is moving in steady state, the stress-velocity relationship determines the drag coefficient. This can

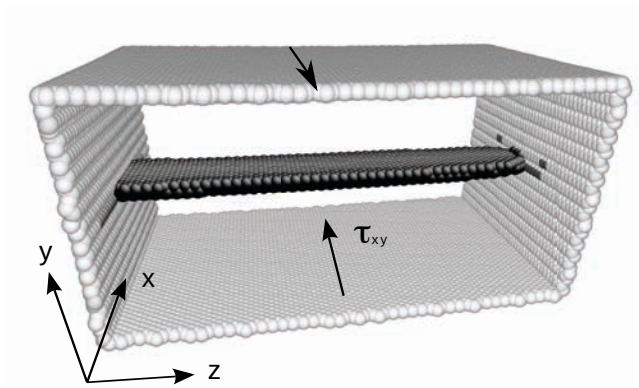

Figure 3.1. An edge dislocation in FCC nickel. The thickness of the thin film is along the y direction and the film (and dislocation length) are along the z direction. Bulk-like simulations are carried out with the z direction under periodic boundary conditions, which are not illustrated here. Reprinted with permission from [72].

be readily obtained from classical molecular dynamics simulations where one applies a constant shear stress and measures the dislocation velocity.

The drag forces which act upon a dislocation are typically caused by the dislocations interactions with either phonons, electrons or magnons. At moderate and high temperatures, the drag caused by electrons can often be ignored. Furthermore, drag by magnons is typically only relevant for magnetic materials. Thus, for most applications, the drag felt by a moving dislocation is caused by the interaction of the line defect with phonons, and is thus typically a thermal drag effect. While numerous theories have been developed to understand dislocation drag [1, 50], they do not lend themselves to systematic investigations of different materials and systems. As just mentioned, classical molecular dynamics can be used to conduct such investigations. However, this approach automatically removes the effects of electron and magnon drag as well as quantum effects of the phonons. Despite these limitations, classical molecular dynamics has proved a useful technique to systematically probe dislocation drag [7, 12, 54].

Here, in an attempt to further understand dislocation motion in confined volumes, we investigate dislocation drag in small volumes. To this end, we create a single dislocation in a thin film, as shown in Figure 3.1 with free surfaces in one dimension and periodic dimensions along the other two. Since such a set up is actually an array of dislocations in a thin film, the volume is increased until the results are independent of system size and thus representative of an isolated dislocation.

The first study aims at determining the effect of the film thickness on drag. Since the thickness of the film was changed to make the results independent of this dimension, which is free, the thickness was then changed from this value to determine an explicit thickness dependence of the thin film. For the numerical results, see Weinberger [71, 72]. What is clear from this in depth study

is that the thickness of the film has little affect on the drag until the thickness is below 5 nm for both the materials modeled (BCC molybdenum and FCC nickel).

Changing the thickness of the film does not introduce any additional free surfaces to the system and thus the changes in drag are either related to fundamental changes in the interactions with the phonons or may be related to buckling in these thin films. If the boundary conditions, along the z-direction in Figure 3.1, is changed from periodic to a free boundary, additional free surfaces are introduced to the simulation. One expects that as the length of the box is increased, the behavior should approach that of a dislocation in the bulk, which is observed. Reducing the length of box (and hence the dislocation) does have an effect on the observed drag behavior. We note that the effective drag coefficient, B, is observed to scale inversely with the dislocation line length [72],

$$B = B_o + \frac{\alpha}{L} \tag{3.2}$$

While altered interactions with phonons could explain the observed increase in drag, there is a more simple logical explanation. The addition of the free surfaces can introduce local surface forces acting on the dislocation line. If we assume these are point forces on the dislocation ends, then force equilibrium over the whole line is:

$$\tau bL = BvL + F^s \tag{3.3}$$

and comparing this to the equilibrium per-unit-length of the dislocation line with an effective drag:

$$\tau bL = B_{\text{eff}} vL \tag{3.4}$$

The By equating these two expressions, an effective drag that scales inversely with the line length, $B_{\text{eff}} = B + \frac{F^s}{vL}$, is obtained. Thus, it seems quite reasonable that the free surfaces are exerting localized forces on the dislocation line that are slowing it down. This could be confirmed by repeating such simulations and measuring the effective drag as with varying amounts of surface roughness. Presumably higher surface roughness will lead to higher localized forces and thus higher effective drag.

These results suggest that such local surface forces, however, are unlikely to be important in understanding the size effects in micro-compression and micro-tension experiments. The changes in drag observed in these simulations don't occur until the system size is below approximately 50 nm. Increased surface roughness will likely increase the magnitude of the forces and thus increase the size range over which the drag is affected. However, given that the micropillar size effect occurs from tens of microns down to a hundred nanometers, it is doubtful that the observed surface forces here will influence the properties significantly for very large pillars.

The Stability of Dislocation Pinning Points

As discussed previously, truncated Frank-Read sources, or spiral arm sources, have been theorized to control plasticity in micro- and sub-micron pillars. This idea is supported by a large number of discrete dislocation dynamics simulations [16, 44, 49, 60, 61, 65, 67]. However, it still remains unclear as to the origin of the hard pinning points assumed in most discrete dislocation dynamics simulations. For example, Motz *et al.* [49] suggest that Lomer-Cottrell segments can act as the strong pinning points in sub-micron pillars. This assumed lack of mobility originates from the immobility of Lomer-Cottrell locks in bulk FCC metals, which is created by the dissociation of the Lomer dislocation onto two different $\{111\}$ planes [43]. However, as pointed out by Lee and Nix [43], it is not immediately clear that these segments will remain immobile as the source arms rotate and that further experiments and atomistic simulations are needed to clarify this point.

In this section we examine the stability of pinning points in nanopillars using molecular dynamics and statics simulations. Specifically, we examine the stability of a variety of pinning points created by Lomer-Cottrell dislocations as suggested by Lee and Nix [43], which we have reported in the literature [73, 76]. This work focuses on determining if Lomer-Cottrell dislocations can pin the dislocations in these small volumes and act as stable single arm sources.

The dislocation sources are created in nanopillars comprised of FCC metals of both nickel and copper modeled as modeled by the Foiles-Hoyt [20] and Mishin [47] EAM potentials. The pillars have an length to diameter aspect ratio of approximately 2:1, a circular cross-section with periodic boundary conditions enforced along the pillar axis. The stability is tested by both minimizing the energy at 0K as well as performing molecular dynamics at 300K under zero applied axial stress. Some stabilities are also tested at 500 MPa and 1 GPa applied axial stresses.

Figure 3.2 shows a typical result of a dislocation source pinned by a Lomer-Cottrell jog. The source is created by a cut-and-weld process and a short minimization is done to remove configurations that are energetically unfavorable. The resulting structure is shown, along with the surface, in Figure 3.2(a). Under an applied axial stress, 1GPa here, the dislocation arms rotate about the Lomer-Cottrell jog as shown in Figure 3.2(b)-(e). The dislocation is able to escape because the Lomer-Cottrell jog is not immobile on its $\{100\}$ plane and is able to drift out of the small pillar volume in short simulation time scales ($\sim$ 100 pico-seconds). Similar behavior is observed if no axial stress is applied, however in that case the dislocation arms do not rotate. We have shown that this is a general trend and the results specifically for Lomer-Cottrell jogs can be found in [73]. Similar observations of dislocation instability were also observed for Lomer-Cottrell dislocations that are not jogs, but rather terminate at the free surface [76].

These simulations [73, 76] illustrate that Lomer-Cottrell structures do not act as strong pinning points. We have also shown that similar but artificially created dislocation segments, such as those that lie on $\{110\}$ and $\{112\}$ planes, also don't act as strong pinning points. The only method found to create a hard pinning point was to trap the dislocations using a cylindrical hole [76].

These simulations illustrate that dislocation junctions, in themselves, may not provide strong enough pinning points in nanopillars as most of the dislocation segments simulated were mobile. However, numerous experiments have reported the operation of single arm sources in FCC metals.

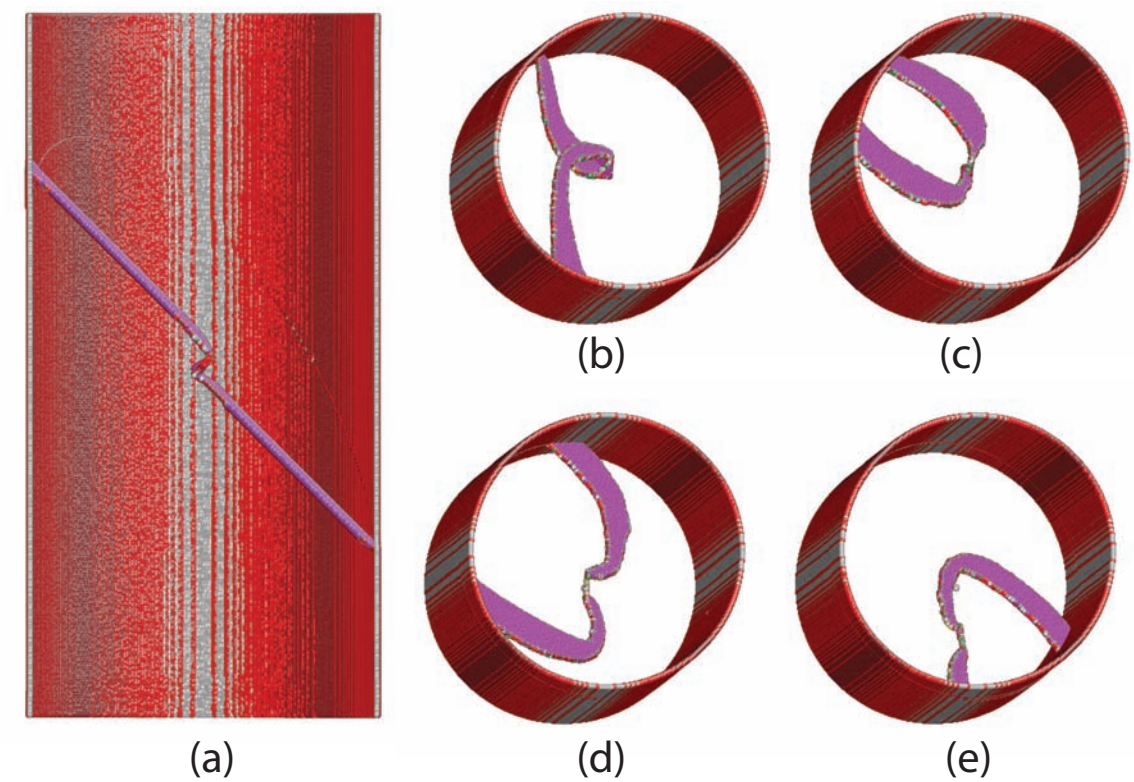

Figure 3.2. A double ended source pinned by a Lomer-Cottrell jog in a 50 nm diameter copper nanopillar. (a) The initial source created by a cut and weld procedure after a short energy minimization. The pillar lies along the $\langle 100 \rangle$ direction in the FCC crystal. The long dislocation segments have a Burgers vector of $\frac{a}{2}\langle 110 \rangle$. The Lomer-Cottrell jog has the same Burgers vector, however, due to its line direction, it must glide on a $\{100\}$ glide plane. (b) Under the applied loads the mobile arms begin to rotate and the Lomer-Cottrell jog dissociates and pins the dislocation. (b)-(c) As the dislocation rotates, the Lomer-Cottrell segment constricts allowing the dislocation to glide on its $\{100\}$ plane and (d) eventually drifts out of the pillar.

Keiner and Minor [34, 35] have observed in their small copper pillars the operation and loss of dislocation sources. While this is in agreement with the simulations performed here, we note the work of Mompiou *et al.* [48] shows the stable operation of a single arm source in their aluminum fibers. This appears, at first glance, to contradict the simulation results reported here. However, the work of Mompiou *et al.* [48] does not report the exact nature of the pinning point in their experiments. Rather than considering the experiments and theory at odds with one another, we can reconcile the two results. Specifically, we can conclude that the pinning points observed in those experiments are not caused by inherent dislocation junction strength, but by some other feature. One possible suggestion is the role of impurities segregating to the dislocation core, pinning the dislocation [73]. While this certainly can pin the dislocation, the possibility of the number of available impurities in these very pure metals may be low. It is also possible that the experimentally determined pinning points are caused by other defects in the crystal such as jogs or vacancies [76].

Chapter 4

Dislocation Nucleation From Free Surfaces

Dislocation nucleation from free surfaces is expected to dominant the plasticity of nanowires and other materials when the dimensions and number of interior defects are reduced. For example, the work of Brenner [8–10] showed that micron-sized whiskers exhibit very high yield strengths followed by low strength flow. Presumably the high yield is a result of the stress required for nucleation while the low flow stress is that required to continue flow. The work by Bei *et al.* [29] also show a very high yield strength in Moly-alloy pillars similar to what was observed in the work by Brenner followed by plastic collapse.

In a similar vein, atomistic simulations have directly shown that in small defect free materials that plasticity is dominated by dislocation emission [14, 55, 56, 74]. These simulations also show a very high yield strength followed by low strength flow. In addition, these simulations have shown that heterogenous dislocation nucleation is temperature and strain rate dependent. The type of plasticity observed in these materials, such as slip via perfect dislocations and deformation twinning appears to be dependent on both wire orientation as well as geometry. These findings, originally predicted by atomistic simulations, are being validated by a number of experiments on pristine nanowires [45, 63, 64, 66, 77, 78, 80].

Recent experiments of the compression of electroplated copper nanopillars by Jennings *et al.* [33] have shown that there appears to be a transition between single arm sources to dislocation nucleation. This is characterized by a change from the power law relationship between the flow stress and diameter to a diameter independent strength plateau. This mechanism was also suggested by previous atomistic simulations [46, 79].

In this section, we investigate both atomistic and continuum models of heterogeneous dislocation nucleation. The end goal is to build a continuum model of dislocation nucleation that is able to predict the transition between the operation of single arm sources and dislocation nucleation. The approach used here is to first compute the energetics of dislocation nucleation using atomistic simulations. With the understanding obtained from the atomistic simulations, continuum models are then developed to predict nucleation in a wide range of materials and crystal orientations.

Atomistics Simulations of Dislocation Nucleation

Using classical nucleation theory, the rate at which a dislocation nucleates can be described using transition state theory as a function of the stress-dependent activation free energy barrier and temperature as:

$$\nu = \nu_o N \exp\left(\frac{-E_b}{k_B T}\right) \tag{4.1}$$

where ν_o is a frequency prefactor, N is the number of nucleation sites, and E_b is the appropriate energy barrier. Thus, the nucleation rate under constant stress or constant strain can be determined from the above equation. However, experiments are conducted under constant strain rate. An implicit expression for the strength can be derived from the survival probability of a nanowire under constant strain rate as [51, 75, 79]

$$\frac{E_b}{k_B T} = \ln\left(\frac{k_B T N \nu_o}{E \dot{\varepsilon} \Omega}\right) \tag{4.2}$$

where $\Omega \equiv -\frac{\partial E_b}{\partial \sigma}$, E is the Young's modulus and $\dot{\varepsilon}$ is the applied strain rate. The nucleation stress can be determined by solving this implicit equation with the knowledge of the stress dependent energy barrier of dislocation nucleation.

To compute this in atomistic simulations, we use gold as a model material as it has been used extensively in both micro-compression experiments [11, 15, 23, 24, 42, 70] and nanowire experiments [45, 64, 66, 78]. Five different geometries were studied: two orientations $\langle 100 \rangle$ and $\langle 110 \rangle$ and three cross sectional geometries: square, circular and rhombic. For more details of the geometry, see [75]

The energy barriers were computed using a free-end string method. The initial state is a pristine nanowire and the final state is the same nanowire with a partial dislocation introduced in it. A sample energy computed for one of the nanowires is shown in Figure 4.1.

From these simulations, the strength of very small, $\sim$5 nm diameter, nanowires can be computed. To predict the strength of much larger nanowires, the data must be corrected for the surface stress. The surface stress adds in a stress that drives nucleation and is inversely proportional to the nanowire diameter [74]. The energy barrier versus stress curves correcting the atomistic data compiled of string method and corrected for the surface stress are shown in Figure 4.2. With the adjustments for the surface stress, one is able to predict the stress of dislocation nucleation in large gold nanowires. Table 4.1 shows the strengths of our nanowires [75] and those of recent experiments [64, 66] showing good agreement.

While the atomistic data shows good agreement with experimental measurements of strength in gold nanowires, it is still desirable to model the transition between single arm sources and surface sources. To this end, we use the atomistic data generated from these energy barrier curves

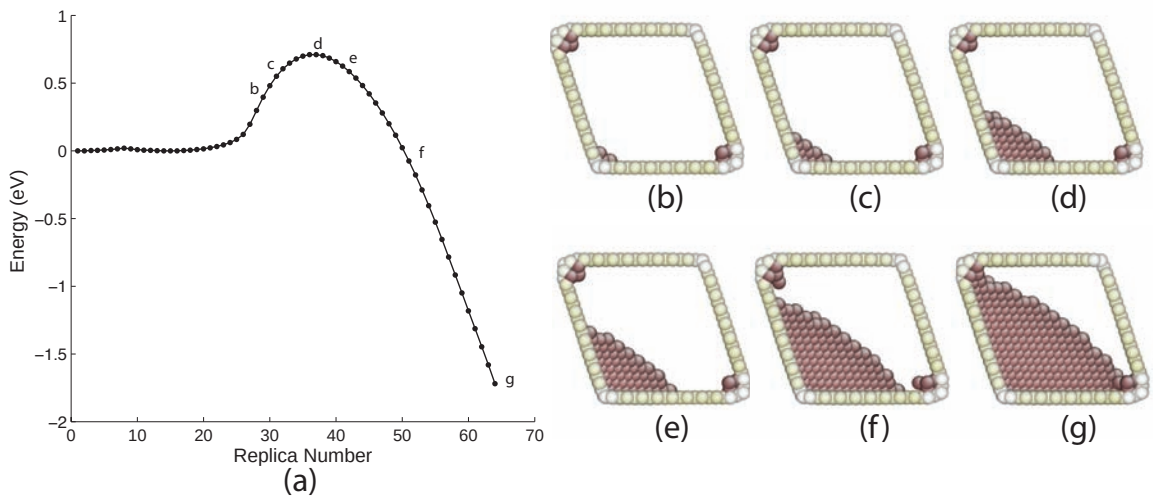

Figure 4.1. (a) The energy barrier and computed for a ~ 5 nm gold nanowire with a rhombic cross-section under a uniaxial compressive stress of approximately 2.6 GPa. (b)-(g) Snapshots of the nucleation process at 2.6 GPa. The subfigure labels correspond to the labels on the curve in (a).

Table 4.1. A comparison of the predicted strengths of large $\sim$ 100 nm diameter gold nanowires as compared to experiments.

Orientation	Loading Direction	cross-section	Theoretical Strength	Experimental Strengths
$\langle 100 \rangle$	tension	$\{100\} \times \{100\}$	1.2 GPa	1.1 GPa [66]
$\langle 110 \rangle$	tension	$\{111\} \times \{111\}$	1.5 GPa	1.54 GPa [66]
$\langle 110 \rangle$	tension	hexahedral	1.5 GPa	0.8-1.6 GPa [64]

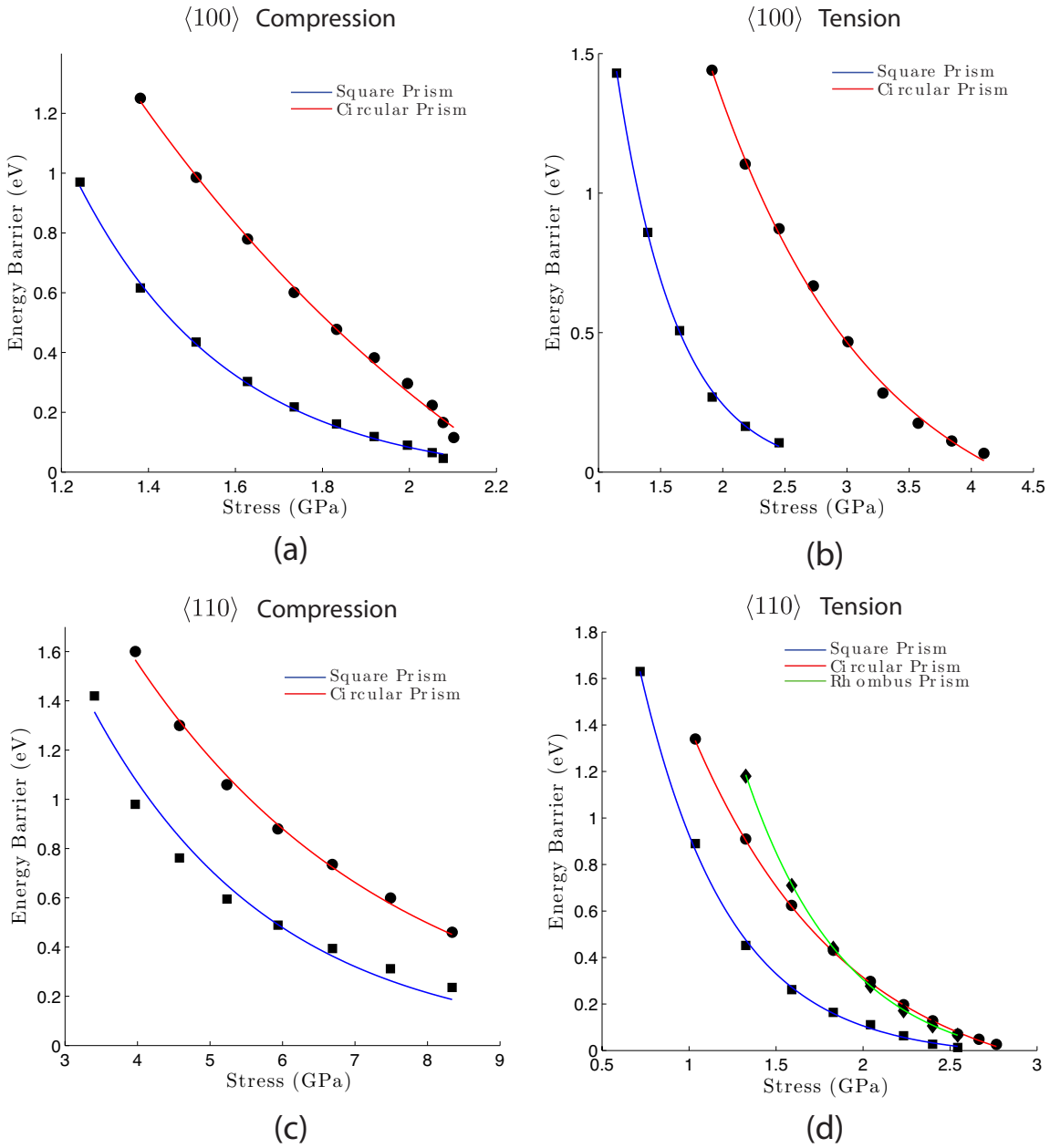

Figure 4.2. The energy barriers of the five different nanowires in tension and compression. (a) Energy barrier curves for the ⟨100⟩ nanowires in compression. (b) Energy barrier curves for the ⟨100⟩ nanowires in tension. (c) Energy barrier curves for the ⟨110⟩ nanowires in compression. (d) Energy barrier curves for the ⟨110⟩ nanowires in tension. Note that the stress values are corrected for the surface stress and are thus representative of large diameter nanowires. The data points represent the data from atomistics and the lines represent curve fits.

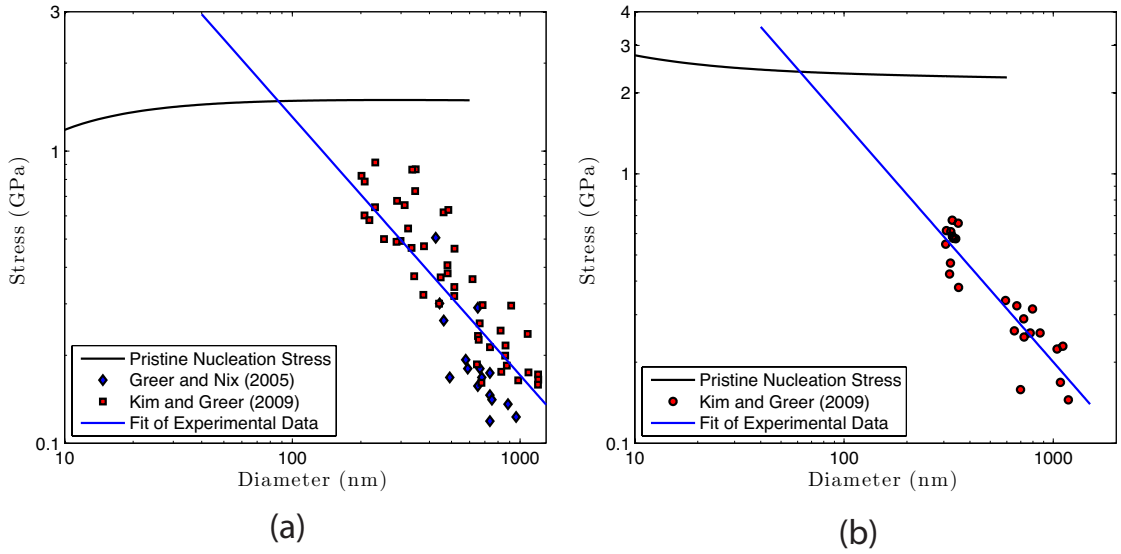

Figure 4.3. The strength predicted from the atomistic simulations as compared against experimental measurements of the flow stress in (a) compression and (a) tension of gold micro- and nano-pillars.

and add in a diameter dependent surface stress to reproduce a surface stress induced size effect. The strength of gold pillars with circular cross-sections with $\langle 100 \rangle$ orientations are then predicted using Equation 4.2 compared with experimental results from micro-tension and micro-compression experiments [24, 37]. We notice a few key results in the predicted size effects of the nucleation strength. First, the surface stress causes a strengthening in tension and weakening in compression and is the dominant contribution to the nucleation size effect. A weaker size effect was suggested by [79] is caused by the number of nucleation sites scaling with the pillar diameter which makes smaller pillars stronger, but this is a weak logarithmic dependence.

Figure 4.3 also nicely illustrates a transition in strength from single arm sources to surface nucleation. We note that the transitions for these $\langle 100 \rangle$ gold nanopillars should occur around 100 nanometers. This is, of course, if one extrapolates the experimental data as is done in Figure 4.3, which may not be appropriate.

Continuum Models for Predicting Nucleation Strengths

In the previous section we used atomistic simulations of energy barriers and transition state theory to predict the nucleation strength of nanowires. This method is advantageous over standard molecular dynamics because it can be extended to strain rates that are experimentally relevant. However, one significant drawback of this method is that it requires the use of atomistic based

energy landscape search methods, such as the string method or the nudged-elastic-band method, to determine the stress-dependent energy barriers. These methods are time consuming and are not amenable to use across a large number of materials and crystal orientations. Furthermore, such models are not practical for use in large-scale defect simulations such as discrete dislocation dynamics. Thus, it is desirable to develop a simple continuum model based on atomistics that is able to easily capture the nucleation energetics.

Bulk Nucleation

Before creating a model of dislocation nucleation from the free surface, we first develop a simple model of homogeneous nucleation. In this work, we follow the method of Aubry *et al.* [2] with a modification of the line energy term that makes the surface nucleation problem easier. This allows us to write the change in free energy of a homogeneously nucleating circular partial dislocation loop as

$$\Delta G = 2\pi R \frac{\mu b_f^2 (2-\nu)}{8\pi(1-\nu)} \ln \frac{R}{r_c} + \pi R^2 \left(\gamma_{GSF}(\tau, u_o + b_f) - \gamma_{GSF}((\tau, u_o)\right) - \pi R^2 \tau b_f \tag{4.3}$$

where R is loop radius, b_f is the magnitude of the dislocation Burgers vector, μ is the shear modulus, ν is Poisson's ratio, τ is the applied shear stress. $\gamma_{GSF}(u)$ is the generalized stacking fault energy, which is a function of the applied stress τ. The value u_o is the displacement obtained when the derivative of the generalized stacking fault energy equals the applied stress, i.e. $\left.\frac{\mathrm{d}\gamma_{GSF(u)}}{\mathrm{d}u}\right|_{u_o} = \tau$.

Atomistic simulations of homogeneous partial dislocation nucleation were also conducted in order to match the two models. The materials modeled in the atomistics are gold, silver, aluminum and nickel. A partial dislocation loop was introduced into a perfect block of material of size $6[111] \times 8[11\bar{2}] \times 13[\bar{1}10]$ and the energy barriers were deterimned using the same method for the gold nanowires. Fitting the model to the atomistic data allows the extraction of the inner core radius, which is shown in Table 4.2. The value for copper was extracted by matching this model to the data of Aubry *et al.* [2]. From this, we can see there is no universal core radius among material models, however the core radius generally lies between the values of $0.5b$ and $0.75b$.

Half Space Nucleation

The nucleation of a dislocation from a half-space is a reliable model of dislocation nucleation from a large diameter pillar. The model assumes the radius of curvature of the nucleating dislocation is much smaller than the pillar diameter, which is a good assumption for pillars of diameters that are around 25 nm or greater at experimental time scales. The model of the free energy for homogeneous nucleation must be modified to account for the free surface. If we restrict our attention to nucleation of circular dislocation loops from a half-space, we note that the line energy compared to homogeneous nucleation is reduced in half. However, the reduction in the line length

Table 4.2. The inner core radius, r_c determined from fitting the model homogeneous partial dislocation nucleation to atomistic data.

Material	r_c
Copper	$0.63b$
Gold	$0.73b$
Silver	$0.50b$
Nickel	$0.63b$
Aluminum	$0.71b$

is not the whole story with regards to the reduction in energy. As shown by Beltz and Freund [6], an additional term must be added inside the logarithm to appropriately modify the energy due to the image stress. Thus, we can write the dislocation elastic energy as:

$$E = \pi R \frac{\mu b_f^2 (2-\nu)}{8\pi(1-\nu)} \ln \frac{mR}{r_c} \tag{4.4}$$

where m is the factor that weakly depends on Poisson's ratio and is approximately 0.55 for a material with a Poisson's ration of 0.3.

To model the uniaxial loading of a nanowire, we have to now use a full stress-tensor dependent stacking fault energy, $\gamma_{GSF}(\sigma)$. Furthermore, the determination of the parameter u_o is now done with the resolved shear stress through the Schmid factor S. Thus, we can write the change in free energy of a nucleating dislocation from a half space under uniaxial loading as

$$\Delta G = \pi R \frac{\mu b_f^2 (2-\nu)}{8\pi(1-\nu)} \ln \frac{mR}{r_c} + \frac{1}{2}\pi R^2 \left(\gamma_{GSF}(\sigma, u_o + b_f) - \gamma_{GSF}((\sigma, u_o)\right) - \frac{1}{2}\pi R^2 \sigma S b_f \tag{4.5}$$

where u_o is determined from the equation $\left.\frac{\mathrm{d}\gamma_{GSF}(u)}{\mathrm{d}u}\right|_{u_o} = S\sigma$. From the change in free energy, the energy barrier as a function of applied axial stress, σ, can be parameterized. The strength can be predicted by assuming the materials are linear elastic, have Young's modulus appropriate for the material and loading orientation, taking ν_o to be the Debye frequency, and N to be a representative number of nucleation sites that scale linearly with the pillar diameter. Since the surface stress introduces a size depenent strength [14, 74], we include a nominal surface stress value of 1 J/m^2, which only affects predictions at small diameters and makes the pillars stronger in tension and weaker in compression.

Figure 4.4 shows a plot of the nucleation strength for a variety of orientations as a function of pillar diameter. Plotted alongside these nucleation strengths is a representative curve of the size-dependent flow strengths of micro- and sub-micronpillars [22, 38, 69]. In this log-log plot, we have normalized the strength using the Schmid factor and shear modulus so that the micropillar

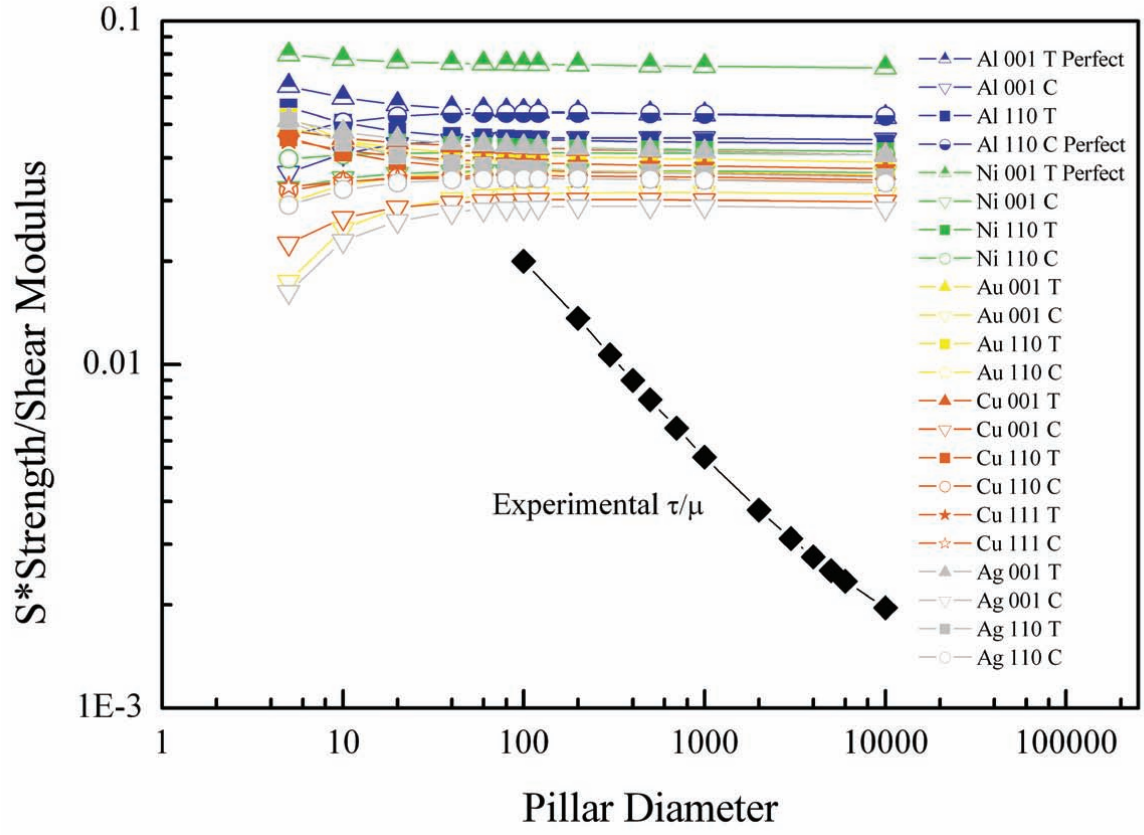

Figure 4.4. The pristine nucleation strength of single crystal FCC metals resolved onto their slip planes compared to the resolved flow strengths from micropillar compression tests.

results exhibit a standard universal form. From these results, we can see that the softer FCC metals, i.e. the noble metals, are the materials that are likely to show a transition from the experimental data, which is governed by the operation of single arm sources, to surface sources. The transitions for nickel and aluminum are much higher. This confirms the notion that nucleation strengths should not follow a universal behavior that is observed for the operation of single arm sources. Furthermore, we note that all of the strengths predicted here fall within a range of $\mu/50$ to $\mu/10$ which are close to the values assumed for the ideal strength.

Chapter 5

Conclusion

In this work, we have developed a number of models for plastic processes in confined volumes. Specifically, we have shown that dislocation drag shows an apparent increase in small volumes, the increase is inversely proportional to the dislocation line length, and is likely caused by localized surface forces. However, the increased resistance to dislocation motion is unlikely to contribute significantly to the experimentally observed size-dependent strength in micropillar compression or tension experiments. This work has also shown that dislocation junctions in nanopillars are unlikely to act as strong pinning points and therefore cannot support prolonged single arm source motion in small volumes alone. The operation of single arm sources observed in experiments could be caused by a number of other defects such as point defects or elementary dislocation jogs. The models of dislocation nucleation showed that atomistic simulations of energy barriers combined with transition state theory can accurately predict the nucleation strength of nanowires. Furthermore, we have shown that the development of continuum based nucleation models can be used to understand the transition points between the operation of single arm sources and surface sources.

As a broader picture, this work shows that atomistic simulations combined with continuum models can be used to gain a better understanding of the plastic processes at the nanoscale. This work has also shown that the two models can be used to develop coarse grained models of plasticity. Such approaches are promising when we look to use small scale mechanical testing to do systematic investigation of mechanical properties.

References

[1] V. I. Alshits and V. L. Indenbom. Mechanisms of dislocation drag. In F. R. N. Nabarro, editor, *Dislocation in Solids*, pages 43–111. North Holland Physics Publishing, 1986.

[2] S. Aubry, K. Kang, S. Ryu, and W. Cai. Energy barrier for homogeneous nucleation: Comparing atomistic and continuum models. *Scripta Mater.*, 64:1043–1046, 2011.

[3] B. Backes, Y. Huang, M. Göken, and K. Durst. The correlation between the internal material length scale and the microstructure in nanoindentation experiments and simulations using the conventional mechanism-based strain gradient plasticity theory. *J. Mater. Res.*, 24:1197–1207, 2009.

[4] C. C. Battaile, B. L. Boyce, C. R. Weinberger, S. V. Prasad, J. R. Michael, and B. G. Clark. The hardness and strength of metal tribofilms: an apparent contradiction between nanoindentation and pillar compression. *Acta Mater.*, 58:1712–1720, 2012.

[5] C. C. Battaile, S. V. Prasad, J. R. Michael, and B. L. Boyce. Mechanical properties of nanocrystalline metal tribofilms. SAND2010-7015, Sandia National Laboratories, 2010.

[6] D. Beltz and L. B. Freund. On the nucleation of dislocations at a crystal surface. *Phys. Stat. Solidi (b)*, 180:303–313, 1993.

[7] E. Bitzek and P. Gumbsch. Atomistic study of drag, surface inertial effects on edge dislocations in face-centered cubic metals. *Mater. Sci. Eng. A*, 387-389:11–15, 2004.

[8] S. S. Brenner. Tensile strength of whiskers. *J. Appl. Phys.*, 27:1484–1491, 1956.

[9] S. S. Brenner. Plastic deformation of copper and silver whiskers. *J. Appl. Phys.*, 28:1023–1026, 1957.

[10] S. S. Brenner. Growth and properties of ”whiskers”. *Science*, 128:569–575, 1958.

[11] S. Brinckmann, J. Y. Kim, and J. R. Greer. Fundamental differences in mechanical behavior between two types of crystals at the nanoscale. *Phys. Rev. Lett.*, 100:155502, 2008.

[12] J. Chang. *Atomistics of defect nucleation and mobility: dislocations and twinning*. PhD thesis, MIT, 2004.

[13] E. Demir, D. Raabe, N. Zaafarani, and S. Zaefferer. Investigate on indentation size effect through the measurement of the geometrically necessary dislocations beneath small indents of different depths using EBSD tomography. *Acta. Mater.*, 57:559–569, 2009.

[14] J. Diao, K. Gall, M. Dunn, and J. Zimmerman. Atomistic simulations of the yielding of gold nanowires. *Acta Mater.*, 54:643–653, 2006.

[15] M. Dietiker, S. Buzzi, G. Pigozzi, J. Löffler, and R. Spolenak. Deformation behavior of gold nano-pillars prepared by nanoimprinting and focused ion-beam milling. *Acta Mater.*, 59:2180–2192, 2011.

[16] J. A. El-Awady, M. Wen, and N. M. Ghoniem. The role of the weakest-link mechanism in controlling the plasticity of micropillars. *J. Mech. Phys. Solids*, 57:32–50, 2009.

[17] N. A. Fleck and J. W. Hutchinson. A phenomenological theory for strain gradient effects in plasticity. *J. Mech. Phys. Solids*, 41:1825–1857, 1993.

[18] N. A. Fleck and J. W. Hutchinson. Strain gradient plasticity. In J. W. Hutchinson and T. Y. Wu, editors, *Advances in Applied Mechanics*, volume 33, pages 296–361. 1997.

[19] N. A. Fleck, G. M. Muller, M. F. Ashby, and J. W. Hutchinson. Strain gradient plasticity: Theory and experiment. *Acta Metall. Mater.*, 42:475–487, 1994.

[20] S. M. Foiles and J. J. Hoyt. Computation of grain boundary stiffness and mobility from boundary fluctuations. *Acta Mater.*, 54:3351–3357, 2006.

[21] H. Gao, Y. Huang, W. D. Nix, and J. W. Hutchinson. Mechanism-based strain gradien plasticity – i. theory. *J. Mech. Phys. Solids*, 47:1239–1263, 1999.

[22] J. Greer and J. de Hosson. Plasticity in small-sized metallic systems: Intrinsic versus extrinsic size effect. *Prog. Mater. Sci.*, 56:654–724, 2011.

[23] J. R. Greer and W. D. Nix. Nanoscale gold pillars strengthened through dislocation starvation. *Phys. Rev. B*, 73:245410, 2006.

[24] J. R. Greer, W. C. Oliver, and W. D. Nix. Size dependence of mechanical properties of gold at the micron scale in the absence of strain gradients. *Acta Mater.*, 52:1821–1830, 2005.

[25] M. D. Guzman, G. Neubauer, P. Flinn, and W. Nix. The role of indentation depth on the measured hardness of materials. *Materials Research Symposium Proceedings*, 308:613–618, 1993.

[26] C.-S. Han, H. Gao, Y. Huang, and W. D. Nix. Mechanism-based strain gradient crystal plasticity–I. theory. *J. Mech. Phys. Solids*, 53:1188–1203, 2005.

[27] C.-S. Han, H. Gao, Y. Huang, and W. D. Nix. Mechanism-based strain gradient crystal plasticity–II. analysis. *J. Mech. Phys. Solids*, 53:1204–1222, 2005.

[28] K. Hattar, L. N. Brewer, B. L. Boyce, T. E. Buchheit, S. M. Foiles, P. Lu, B. G. Clark, P. G. Kotula, S. Goods, J. Puskar, and B. L. Doyle. Fast neutron environments. SAND2011-8527, Sandia National Laboratories, 2011.

[29] H.Bei, S. Shim, M. Miller, E. George, and G. Pharr. Compressive strengths of molybdenum alloy micro-pillars prepared using a new technique. *Scripta Mater.*, 57:397–400, 2007.

[30] H.Bei, S. Shim, G. Pharr, and E. George. Effects of pre-strain on the compressive stress-strain response of mo-alloy single-crystal micropillars. *Acta Mater.*, 56:4762–4770, 2009.

[31] Y. Huang, H. Gao, W. D. Nix, and J. W. Hutchinson. Mechanism-based strain gradient plasticity–II. analysis. *J. Mech. Phys. Solids*, 48:99 – 128, 2000.

[32] A. T. Jennings, M. J. Burek, and J. R. Greer. Microstructure versus size: Mechanical properties of electroplated single crystalline cu nanopillars. *Phys. Rev. Lett.*, 104:135503, 2010.

[33] A. T. Jennings, J. Li, and J. R. Greer. Emergence of strain rate effects in cu nano-pillars: Transition from dislocation multiplication to dislocation nucleation. *Acta Mater.*, 59:5627–5637, 2011.

[34] D. Kiener and A. M. Minor. Source-controlled yield and hardening of cu (1 0 0) studied by in situ transmission electron microscopy. *Acta Mater.*, 59:13281337, 2011.

[35] D. Kiener and A. M. Minor. Source truncation and exhaustion: Insights from quantitative in situ tem tensile testing. *Nano Letters*, 11:38163820, 2011.

[36] D. Kiener, R. Pippan, C. Motz, and H. Kreuzer. Microstructural evolution of the deformed volume beneath microindents in tungsten and copper. *Acta. Mater.*, 54:2801–2811, 2006.

[37] J.-Y. Kim and J. Greer. Tensile and compressive behavior of gold and molybdenum single crystals at nano-scale. *Acta. Mater.*, 57:5245–5253, 2009.

[38] O. Kraft, P. A. Gruber, R. Monig, and D. Weygand. Plasticity in confined dimensions. *Annual Rev. Mater. Res.*, 40:293–317, 2010.

[39] H. Kreuzer and R. Pippan. Discrete dislocation simulation of nanoindentation: Indentation size effect and the influence of slip band orientation. *Acta. Mater.*, 55:3229–3235, 2007.

[40] L. P. Kubin and A. Mortensen. Geometrically necessary dislocations and strain-gradient plasticity: a few critical issues. *Scripta Mater.*, 48:119–125, 2003.

[41] S. Lee, S. Han, and W. Nix. Uniaxial compression of fcc au nanopillars on an MgO substrate: The effects of prestraining and annealing. *Acta Mater.*, 57:4404–4415, 2009.

[42] S.-W. Lee, S. Aubry, W. D. Nix, and W. Cai. Dislocation junctions and jogs in a free-standing fcc thin film. *Modell. Simul. Mater. Sci. Eng.*, 19:025002, 2011.

[43] S.-W. Lee and W. D. Nix. Geometrical analysis of 3d dislocation dynamics simulations of fcc micro-pillar plasticity. *Mater. Eng. Sci. A*, 527:1903–1910, 2010.

[44] Z. Liu, X. Liu, Z. Zhuang, and X. You. Atypical three-stage-hardening mechanical behavior of cu single-crystal micropillars. *Scripta Mater.*, 60:594–597, 2009.

[45] Y. Lu, J. Song, J. Y. Huang, and J. Lou. Fracture of Sub-20nm Ultrathin Gold Nanowires. *Advanced Functional Materials*, 21(20):3982–3989, 2011.

[46] J. Marian and J. Knap. Breakdown of self-similar hardening behavior in au nanopillar microplasticity. *International Journal for Multiscale Computational Engineering*, 5:287–294, 2007.

[47] Y. Mishin, D. Farkas, M. J. Mehl, and D. A. Papaconstantopoulos. Interatomic potentials for monoatomic metals from experimental data and *ab initio* calculations. *Phys. Rev. B*, 59:3393–3407, 1999.

[48] F. Mompiou, M. Legros, A. Sedlmayr, D. Gianola, D. Caillard, and O. Kraft. Source based strengthening of sub-micrometer al fibers. *Acta Mater.*, 5:997–1096, 2012.

[49] C. Motz, D. Weygand, J. Senger, and P. Gumbsch. Initial dislocation structures in 3-d discrete dislocation dynamics and their influence on microscale plasticity. *Acta Mater.*, 57:1744–1754, 2009.

[50] E. M. Nadgorny. Dislocation dynamics and mechanical properties of crystals. *Prog. Mater. Sci.*, 31:1–530, 1988.

[51] A. Ngan, L. Zhuo, and P. Wo. Size dependence and stochastic nature of yield strength of micron-sized crystals: a case study on Ni3Al. *Proc. R. Soc.*, 462:1661–1681, 2006.

[52] W. Nix and H. Gao. Indentation size effects in crystalline materials: a law for strain gradient plasticity. *J. Mech. Phys. Solids*, 46:411–425, 1998.

[53] W. Nix and S. Lee. Micro-pillar plasticity controlled by dislocation nucleation at surfaces. *Philos. Mag.*, 91:1084–1096, 2011.

[54] D. L. Olmstead, L. G. Hector Jr., W. A. Curtin, and R. J. Clifton. Atomistic simulations of dislocation mobility in Al, Ni and Al/Mg alloys. *Modell. Simul. Mater. Sci. Eng.*, 13:371–388, 2005.

[55] H. S. Park, K. Gall, and J. Zimmerman. Deformation of fcc nanowires by twinning and slip. *J. Mech. Phys. Solids*, 54:1862–1881, 2006.

[56] H. S. Park and J. A. Zimmerman. Modeling inelasticity and failure in gold nanowires. *Phys. Rev. B*, 72:054106, 2005.

[57] T. A. Parthasarathy, S. I. Rao, D. M. Dimiduk, M. D. Uchic, and D. R. Trinkle. Contribution to size effect of yield strength from the stochastics of dislocation source lengths in finite samples. *Scripta Mater.*, 56:313–316, 2007.

[58] G. M. Pharr, E. G. Herbert, and Y. Gao. The indentation size effect: A critical examination of experimental observations and mechanistic interpretations. *Annual Rev. Mater. Res.*, 40:271–292, 2010.

[59] S. Prasad, C. Battaile, and P. Kotula. Friction transitions in nanocrystalline nickel. *Scripta Mater.*, 64:729–732, 2011.

[60] S. Rao, D. Dimiduk, T. Parthasarathy, M. Uchic, M. Tang, and C. Woodward. Athermal mechanisms of size-dependent crystal flow gleaned from three-dimensional discrete dislocation simulations. *Acta Mater.*, 56:3245–3259, 2008.

[61] S. Rao, D. Dimiduk, M. Tang, M. Uchic, T. Parthasarathy, and C. Woodward. Estimating the strength of single-ended dislocation sources in micron-sized single crystals. *Philos. Mag.*, 87:4777–4794, 2007.

[62] M. Rester, C. Motz, and R. Pippan. Microstructural investigation of the volume beneath nanoindentions in copper. *Acta. Mater.*, 55:6427–6435, 2007.

[63] G. Richter, K. Hillerich, D. Gianola, R. Monig, O. Kraft, and C. Volkert. Ultrahigh strength single crystalline nanowhiskers grown by physical vapor deposition. *Nano Lett.*, 9:3048–3052, 2009.

[64] A. Sedlmayr, E. Bitzek, D. S. Gianola, G. Richter, R. Moenig, and O. Kraft. Existence of two twinning-mediated plastic deformation modes in Au nanowhiskers. *Acta Mat.*, 60:3985–3993, 2012.

[65] J. Senger, D. Weygand, P. Gumbsch, and O. Kraft. Discrete dislocation simulations of the plasticity of micro-pillars under unaxial loading. *Scripta Mater.*, 58:587–590, 2008.

[66] J.-H. Seo, Y. Yoo, N.-Y. Park, S.-W. Yoon, H. Lee, S. Han, S.-W. Lee, T.-Y. Seong, S.-C. Lee, K.-B. Lee, P.-R. Cha, H. S. Park, B. Kim, and J.-P. Ahn. Superplastic deformation of defect-free au nanowires via coherent twin propagation. *Nano Lett.*, 11:34993502, 2011.

[67] H. Tang, K. W. Schwarz, and H. D. Espinosa. Dislocation-source shutdown and the plastic behavior of single-crystal micropillars. *Phys. Rev. Lett.*, 100:185503, 2008.

[68] M. D. Uchic, D. M. Dimiduk, J. N. Florando, and W. D. Nix. Sample dimensions influence strength and crystal plasticity. *Science*, 305:986–989, 2004.

[69] M. D. Uchic, P. A. Shade, and D. Dimiduk. Plasticity of micrometer-scale single crystals in compression. *Annual Rev. Mater. Res.*, 39:361–386, 2009.

[70] C. Volkert and E. Lilleodden. Size effects in the deformation of sub-micron au columns. *Philos. Mag.*, 86:5567–5579, 2006.

[71] C. R. Weinberger. A comment on ”lattice resistance to dislocation motion at the nanoscale”. *Phys. Rev. Lett.*, 105:099601, 2010.

[72] C. R. Weinberger. Dislocation drag at the nanoscale. *Acta Mater.*, 58:6535–6541, 2010.

[73] C. R. Weinberger and W. Cai. The stability of Lomer-Cottrell jogs in nanopillars. *Scripta Mater.*, 64:529–532, 2011.

[74] C. R. Weinberger and W. Cai. Plasticity of metal nanowires. *J. Mater. Chem.*, 22:3277–3292, 2012.

[75] C. R. Weinberger, A. T. Jennings, K. Kang, and J. R. Greer. Atomistic simulations and continuum modeling of dislocation nucleation and strength in gold nanowires. *J. Mech. Phys. Solids*, 60:84–103, 2012.

[76] C. R. Weinberger and G. J. Tucker. Atomistic simulations of dislocation pinning points in pure face-centered-cubic nanopillars. *Model. Simul. Mater. Sci. Eng.*, 20:075001, 2012.

[77] Y. Yue, P. Liu, Z. Zhang, X. Han, and E. Ma. Approaching the Theoretical Elastic Strain Limit in Copper Nanowires. *Nano Lett.*, 11:3151–3155, 2011.

[78] H. Zheng, A. Cao, C. R. Weinberger, J. Y. Huang, K. Du, J. Wang, Y. Ma, Y. Xia, and S. X. Mao. Discrete plasticity in sub-10-nm-sized gold crystals. *Nature Commun.*, 1:144, 2010.

[79] T. Zhu, J. Li, A. Samanta, A. Leach, and K. Gall. Temperature and strain-rate dependence of surface dislocation nucleation. *Phys. Rev. Lett.*, 100:025502, 2008.

[80] Y. Zhu, Q. Qin, F. Xu, F. Fan, Y. Ding, T. Zhang, B. J. Wiley, and Z. L. Wang. Size effects on elasticity, yielding, and fracture of silver nanowires: *In situ* experiments. *Phys. Rev. B*, 85:045443, Jan 2012.

DISTRIBUTION:

1	MS 1411	Amy C. Sun, 1814
1	MS 1411	Stephen M. Foiles, 1814
1	MS 0889	Corbett C. Battaile, 1814
1	MS 1411	Hojun Lim, 1814
1	MS 1411	Garritt J. Tucker, 1814
1	MS 0889	Brad L. Boyce, 1831
1	MS 0878	R. Allen Roach, 2735
1	MS 9404	Jonathan A. Zimmerman, 8256
1	MS 0899	Technical Library, 9536 (electronic copy)
1	MS 0359	D. Chavez, LDRD Office, 1911

Sandia National Laboratories